Chemistry Europe
European Chemical Societies Publishing

Supramolecular Chemistry

Discordant Supramolecular Fibres Reversibly Depolymerised by Temperature and Light

Marieke Gerth,[a, b, c, d] José Augusto Berrocal,[e] Davide Bochicchio,[f] Giovanni M. Pavan,[f, g] and Ilja K. Voets*[a, c]

Abstract: Synthetic stimuli responsive supramolecular polymers attract increasing interest for their ability to mimic the unique properties of natural assemblies. Here we focus on the well-studied benzene-1,3,5-tricarboxamide (BTA) motif, and substitute it with two (*S*)-3,7-dimethyloctyl groups and an azobenzene photoswitch. We demonstrate the UV ($\lambda =$ 365 nm) induced depolymerisation of the helical hydrogen-bonded polymers in methylcyclohexane (MCH) through circular dichroism and UV-vis spectroscopy in dilute solution (15 μM), and NMR and iPAINT super-resolution microscopy in concentrated solution (300 μM). The superstructure can be regenerated after thermal depolymerization, whilst repeated depolymerisation can be reversed without degradation by irradiating at $\lambda = 455$ nm. Molecular dynamics simulations show that the most energetically favourable configuration for these polymers in MCH is a left-handed helical network of hydrogen-bonds between the BTA cores surrounded by two right-handed helices of azobenzenes. The responsiveness to two orthogonal triggers across a broad concentration range holds promise for use in, for example, photo-responsive gelation.

Introduction

Supramolecular chemistry offers a broad palette of handles to fine-tune the hierarchical nanostructure and associated properties of materials through the strong dependence of the configuration of supramolecular assemblies on external variables and exact chemical structure of the monomers.[1] By incorporating selected chemical groups into supramolecular moieties, the responsivity of supramolecular constructs to specific external cues can thus be extended by design.[2] Being able to reversibly switch between a material with and without emerging properties, especially through local (de)activation, is a continuous quest in material science that is being tackled from the molecular to the macro-scale.[3]

In contrast to, for example, thermal cues, light can easily be applied in a patterned fashion to achieve localised responses in a non-invasive fashion.[3a,4] Numerous light-responsive systems based on supramolecular assembly have been presented in the past years, which upon irradiation can, e.g., covalently polymerise,[5] undergo supramolecular polymerisation upon release of protons from a photo-acid,[6] change "secondary structure" of the backbone,[2a] catastrophically depolymerise due to strain build-up,[7] or act as nanoscopic switches for macroscopic actuation.[3c,8] Synthetic accessibility of azobenzenes and re-

[a] *Dr. M. Gerth, Prof. Dr. I. K. Voets*
Self-Organizing Soft Matter group
Faculty of Chemical Engineering and Chemistry
Eindhoven University of Technology
Groene Loper 3, 5612AE Eindhoven (The Netherlands)
E-mail: i.voets@tue.nl

[b] *Dr. M. Gerth*
Laboratory of Physical Chemistry
Faculty of Chemical Engineering and Chemistry
Eindhoven University of Technology
Groene Loper 3, 5612AE Eindhoven (The Netherlands)

[c] *Dr. M. Gerth, Prof. Dr. I. K. Voets*
Institute for Complex Molecular Systems
Eindhoven University of Technology
Groene Loper 3, 5612AE Eindhoven (The Netherlands)

[d] *Dr. M. Gerth*
Van't Hoff Laboratory for Physical and Colloid Chemistry
Debye Institute for Nanomaterials Science
Utrecht University
Padualaan 8, 3584CH Utrecht (The Netherlands)

[e] *Dr. J. A. Berrocal*
Adolphe Merkle Institute
University of Fribourg
Chemin des Verdiers 4, 1700 Fribourg (Switzerland)

[f] *Dr. D. Bochicchio, Prof. Dr. G. M. Pavan*
Department of Innovative Technologies
University of Applied Sciences and Arts of Southern Switzerland
Galleria 2, Via Cantonale 2c, 6928 Manno (Switzerland)

[g] *Prof. Dr. G. M. Pavan*
Department of Applied Science and Technology
Politecnico di Torino
Corso Duca degli Abruzzi 24, 10129 Torino (Italy)

Supporting information and the ORCID identification number(s) for the author(s) of this article can be found under: https://doi.org/10.1002/chem.202004115.

lated light-responsive molecular switches allows targeted design of photoswitches that are responsive to light of different wavelengths.[9]

A supramolecular construct that has been studied extensively, both experimentally[10] and computationally,[11] is the synthetically accessible benzene-1,3,5-tricarboxamide (BTA) motif. Such BTAs can form temperature-responsive supramolecular structures in certain solvents and are versatile supramolecular building blocks, since they can be designed for self-assembly in aqueous environments[11b,12] or apolar alkane solvents.[10b,13] Here, inspired by previous work on azobenzene-decorated BTAs,[3b,14] we synthesise a BTA derivative (Figure S1, S5, S9, S13) comprising an azobenzene as a molecular photoswitch (azoBTA, Figure 1) for light-induced cycling between an associated and dissociated state in apolar solvents such as methylcyclohexane (MCH). We show through a combination of spectroscopic experiments on dilute solutions (15 μM), and NMR and super-resolution microscopy on concentrated solutions (300 μM) that the photoisomerisation and (dis)association is reversible and occurs over a broad range of concentrations. It should be noted that the above-mentioned azobenzene-decorated BTAs are C_3-symmetrical, whereas the azoBTA presented here is not. The desymmetrisation is expected to influence the (light-induced de-)polymerisation, as well as the structure of the fibres. We indeed find that the helices formed by the hydrogen bonds are left-handed, whereas the helices formed by the azobenzene-bearing moieties are predominantly right-handed, yielding a discordant helical structure.

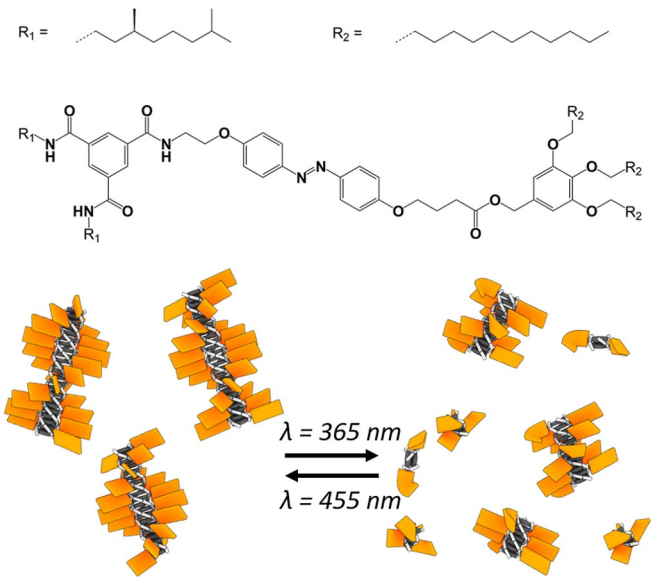

Figure 1. Chemical structure of azobenzene functionalised BTA and a cartoon representation of their discordant superstructure and light-induced dissociation. In the cartoon the benzene rings of the BTA cores are indicated as black disks, the hydrogen bonds are depicted in white, and the azobenzenes are represented by the orange rectangles. *Trans*-azobenzenes are flat rectangles, whereas *cis*-azobenzenes are slightly twisted rectangles. Irradiation with light of $\lambda = 365$ nm (λ_{365nm}) leads to (partial) depolymerisation of the equilibrated discordant fibres, which is reversible through irradiation at $\lambda = 455$ nm or thermal relaxation.

Results and Discussion

AzoBTA forms H-bond stabilised polymers in methylcyclohexane

First, we investigate spectroscopically whether azoBTA molecules are able to form helical superstructures when the azobenzene is present in the side chain of the monomer structure. The UV-vis absorption at $200 \leq \lambda \leq 275$ nm originates from the BTA core (Figure 2A).[15] The *trans*-azobenzene moieties absorb between $\lambda \approx 300$–400 nm, and the low-intensity UV-vis absorption peak above $\lambda \approx 420$ nm is attributed to *cis*-azobenzene. This is a minority species (Figure S14) in the thermodynamic equilibrium distribution at 20 °C, but exhibits an unexpectedly strong Cotton effect in circular dichroism (CD) spectroscopy (Figure 2A). The CD spectrum of azoBTA in MCH exhibits a strong negative signal centred around $\lambda = 225$ nm, which is attributed to the preferred left-handed helical assembly of γ-(*S*)-BTA (Figure 2A).[10b,16] The positive CD signal originating from the azobenzene units indicates that also these are helically arranged. In the Fourier Transform Infrared (FTIR) spectra, we observe characteristic vibrational peaks for non-hydrogen-bonded species ($\nu = 3450$ cm^{-1} and 1666 cm^{-1}) in $CHCl_3$—a solvent wherein azoBTA is molecularly dissolved—which shift to lower wavenumbers in MCH ($\nu = 3238$ cm^{-1} and 1642 cm^{-1}), indicative for hydrogen-bond formation (Figure 2B).[10b,17] We record the variable temperature (VT)-UV-vis and CD (Figure 2C and S17) spectra of 15 μM azoBTA in MCH to find the melting temperature of the azoBTA polymers. The red-shifted UV-vis absorption shoulder of the *trans*-azobenzene peak at low temperature indicates the presence of J-type aggregates, which are aggregates characterised by a large angular offset.[18] Upon heating above the melting temperature of the fibres ($T_m \approx 75$ °C), the vanishing CD signal for both the BTA and azobenzene chromophores indicates that azoBTA is molecularly dissolved (Figure 2C). Supramolecular assembly into one-dimensional fibres is confirmed by small-angle X-ray scattering (SAXS). We obtain for 3 mM azoBTA in MCH a core radius of 13.8 Å and a thickness of 19.0 Å using a core–shell cylinder model[31] to describe the SAXS profile (Figure 2D). The length of the fibres is too long to resolve.

Molecular dynamics simulations provide an insight into the internal structure

Intrigued by the fact that the CD spectra seem to suggest the presence of opposite helicities for the BTA cores and azobenzene units, we performed all-atom molecular dynamics (MD) simulations to investigate the internal arrangement of the azoBTA fibres at atomistic resolution. We built an atomistic model of the azoBTA monomer and parametrised it in the framework of GAFF (General Amber Force Field),[20] as previously done for other BTA variants[11b,21] and other azo-containing self-assembling monomers.[7,22] Then, we constructed a model fibre composed of 30 initially extended azoBTA monomers arranged in 4 different ways (generating 4 different starting configurations for the fibres, see Figure 3a), spanning through the

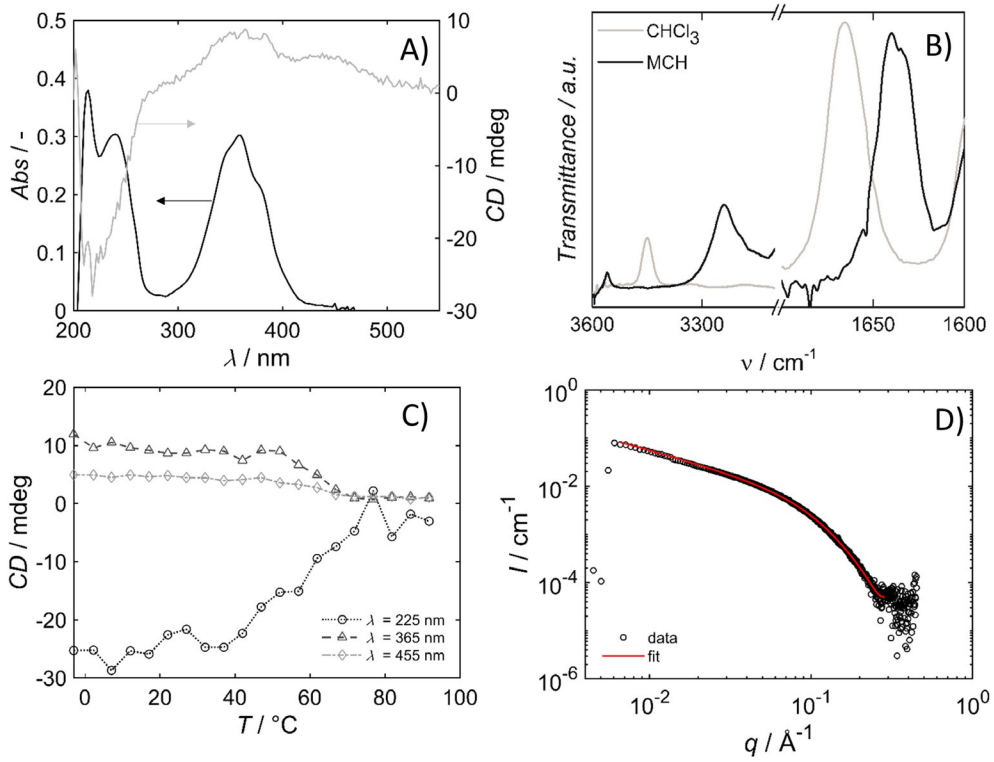

Figure 2. AzoBTA forms H-bond stabilised polymers in methylcyclohexane. A) A representative UV-vis absorption and CD spectrum of azoBTA at 15 μM in MCH at 20 °C. The absorption peak originating from the (hydrogen bonded) BTA is in the range $200 \leq \lambda \leq 275$ nm, from *trans*-azobenzene between $\lambda = 300$–400 nm, and from *cis*-azobenzene above ≈420 nm. B) FTIR spectroscopy shows signature peaks at $\nu = 3238$ cm^{-1} and 1642 cm^{-1} for hydrogen-bonded BTAs at 500 μM in MCH, and monomers at 500 μM in $CHCl_3$. C) Evolution of CD signal at diagnostic wavelengths for BTA ($\lambda = 225$ nm), *trans*-azobenzene ($\lambda = 365$ nm) and *cis*-azobenzene ($\lambda = 455$ nm) assembly with temperature. The concentration of azoBTA is 15 μM in MCH. The temperature was increased at 10 °C h^{-1}, and the sample was kept isothermal during the measurements of the spectra. D) The SAXS profile (open circles) of a 3 mM sample in MCH and fit (line) match a core–shell cylindrical structure.[19]

simulation box through periodic boundary conditions (PBC) to effectively model a portion of the bulk of infinite supramolecular polymers. Among the four initial configurations, two have concordant (the same) helicities for the hydrogen bonds involving the amide groups of the BTA monomers and the stacking of the azobenzene groups (S1 and S3), and two have discordant (opposite) helicities between BTA and azobenzenes (S2 and S4). Two configurations have a single azobenzene helix (S2 and S3) and two have a double helical structure (S1 and S4), see Figure 3a. In all cases, we solvated the initially extended fibre models with the same quantity (4000) of explicit MCH solvent molecules. These models have then been relaxed and equilibrated through 400 ns of MD simulations conducted in NPT conditions (constant N: number of particles, P: pressure and T: temperature during the run) at the temperature of 300 K and 1 atm of pressure. During this time all systems were seen to equilibrate in the MD regime. Then, we compared the last 200 ns (equilibrated part) of each MD simulation.

As a common feature in all four cases we could observe that during the MD simulations the fibres deviate quite a lot from their initially extended configuration, while at the same time these substantially preserve the order in terms of stacking of the BTA cores (see Supporting Figure S18: *g(r)* between the BTA cores). The average number of H-bonds per BTA monomer is in every case around ≈2.5. This indicates a relatively high stability and order of the stacking of the BTA cores, which is preserved in a better way than in BTA variants designed to self-assemble in water, where we previously found a value of around ≈2.1 (as seen recently, the maximum of 3 H-bonds per-monomer is not reached in these systems in solution due to thermal oscillations/vibrations and deviations from perfection).[11a,b,21–22] Compared to the BTA cores, we observe that the order in the helical arrangement of the azobenzene units is much more impaired.

From these MD simulations, we can also compare the different fibre structures in terms of interactions between the monomers in the assembly as well as with the external solvent. From an energy point of view, the simulations suggest that the best arrangement for the azoBTA fibre is a double azobenzene helix discordant with respect to the inner H-bond architecture (S4: see Figure 3a). In fact, the S4 arrangement minimises both the total potential energy of the system (Figure 3c: sum of solute-solute, solute-solvent and solvent-solvent interactions) and in particular the azoBTA–azoBTA monomer–monomer interaction energy (see Supporting Figure S19), while the other 3 configurations are relatively higher in energy (and quite similar between them). We decomposed the azoBTA-azoBTA interaction energy in 4 different terms, as shown in Figure 3c, in order to investigate the major driving force for this difference. Namely, we decomposed the monomer-mono-

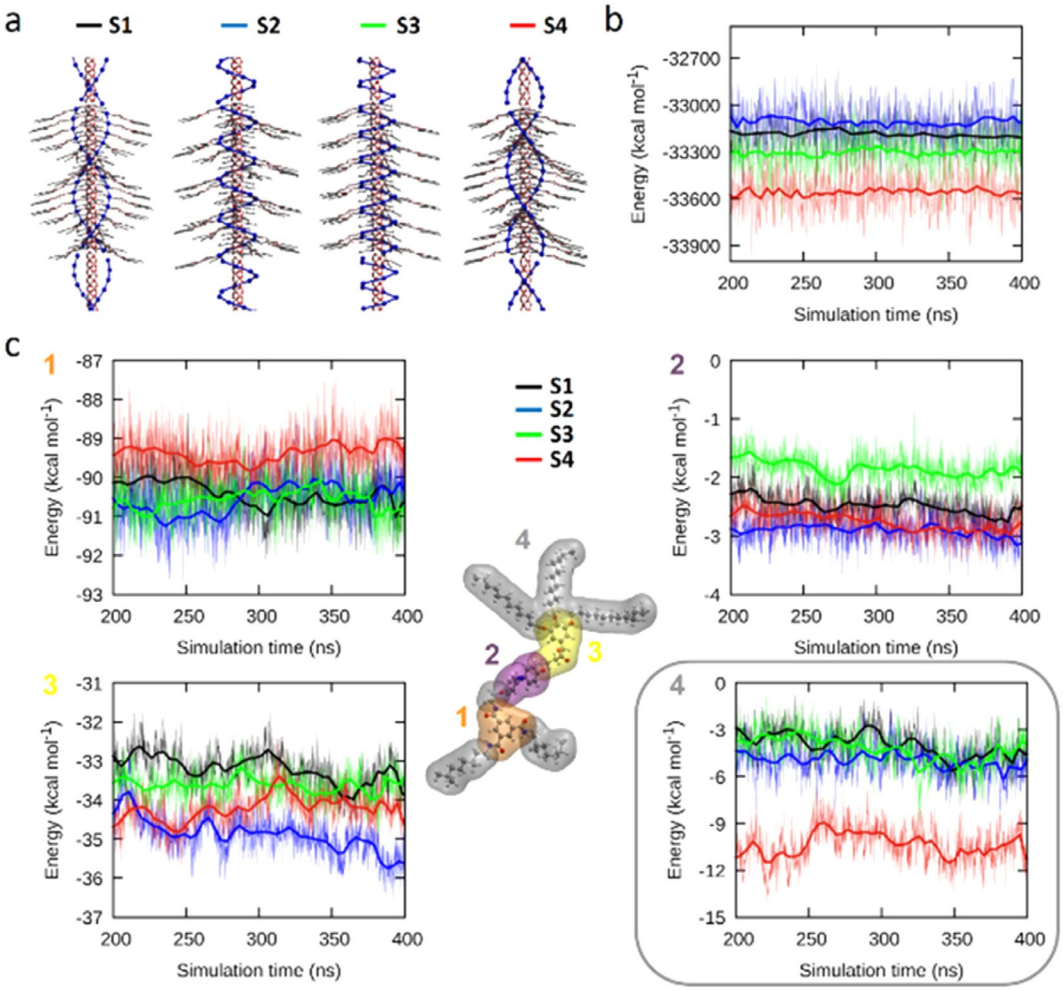

Figure 3. Molecular dynamics simulations. a) The four different initial azoBTA arrangements used in this work: S1 and S3 have concordant helicities between the amides H-bonding (in red) and azobenzene stacking (in blue), while S2 and S4 have discordant helicities. b) Total potential energy in the systems (sum of the total solute-solute, solute-solvent and solvent-solvent interactions) taken from the equilibrated part (last 200 ns) of MD—this is minimized in the S4 assembled structure. c) Decomposition of the azoBTA-azoBTA interaction energy (values per-monomer): core-core (1: orange), azobenzene-azobenzene (2: purple), polar group-polar group (3: yellow) and alkyl chain-alkyl chain (4: grey).

mer interaction energy in terms of how much of this is due to the monomer cores, tails, etc. (data and Scheme in Figure 3c: how much the cores interact between themselves, the tails between themselves, etc.; energy values expressed per monomer). We find that, in general, the core-core interaction (Figure 3c: **1**, orange plot) is much more relevant than the azobenzene-azobenzene interaction (**2**, purple plot) for the monomer–monomer interaction energy, which is consistent with the evidence that during the MD simulations on average the core–core stacking is preserved to a higher extent compared to that between the azobenzene units. S2 and S4, the configurations in which the helicities are opposed, are the ones that minimise the azobenzene–azobenzene interaction (Figure 3c: **2**, purple plot). However, from the decomposition analysis, it becomes clear that the higher stability of S4 comes mainly from the optimisation of the interactions between carbon chains (Figure 3c: **4**, grey plot), which is found about 8 kcal mol^{-1} more favourable than in the other cases. Interestingly, S4 is also the system in which the azobenzene-azobenzene displacement and aggregation differs more compared to the others (Supporting Figure S20: higher *g(r)*, indicating a stronger compaction of azobenzene moieties). In S4 the azobenzene moieties are more compactly arranged due to the stronger folding and interaction of the alkyl chains. Altogether, the MD results indicate that at $T = 300$ K these azoBTA monomers prefer to form a 1D stack with opposed helicities for BTAs and azobenzenes. From an energy point of view, this is thus suggested to be the most favourable, and thus likely, the structure which these assemblies adopt in solution under the experimental conditions.

Reversible photoisomerisation

With the confirmation that the supramolecular polymers melt at high temperatures and after establishing the most likely conformation of the polymers in solution, we study the photoresponsivity of the motifs. We investigate the addressability of the azobenzenes with UV light (λ_{365nm}) through ^{1}H NMR experiments (Figure 4) on a model compound azoBTA-CO_2Et (Fig-

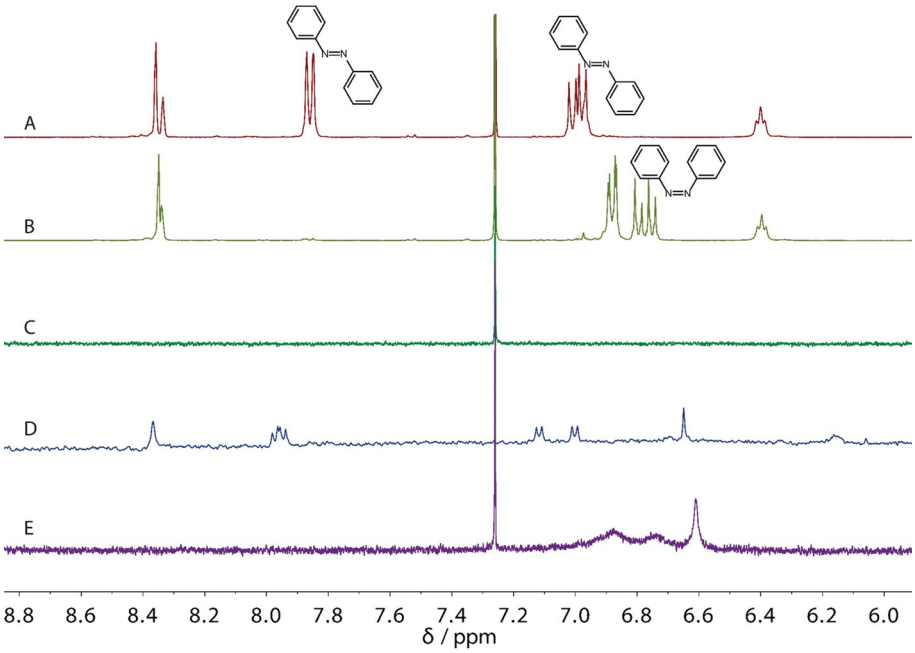

Figure 4. ^{1}H NMR spectra of azoBTA and a model compound azoBTA-CO_2Et under various conditions. ^{1}H NMR spectrum of 300 μM azoBTA-CO2Et A) before irradiation in $CDCl_3$, and B) irradiated with λ_{365nm} in $CDCl_3$. ^{1}H NMR spectrum of 300 μM azoBTA C) before irradiation in d_{14}-MCH at room temperature, D) before irradiation in d_{14}-MCH at $T = 75\,^\circ$C, and E) irradiated with λ_{365nm} in d_{14}-MCH. Irradiation was performed for 15 min at 600 mA.

ure S21) in deuterated chloroform ($CDCl_3$), and next investigate the light response of the assembled azoBTA in deuterated MCH (d_{14}-MCH). A model compound was used in $CDCl_3$ due to the limited availability of azoBTA; since there is no self-assembly in chloroform, we are confident it would have the same isomerisation behaviour. We focus on the aromatic region (chemical shifts $8.9 < \delta < 5.9$ ppm), which is where the diagnostic peaks originating from the hydrogens of the aromatic rings of the azobenzene appear. A comparison of the ^{1}H NMR spectra in $CDCl_3$ at room temperature for monomeric azoBTA before (Figure 4A) and after (Figure 4B) irradiation with λ_{365nm} reveals a characteristic doublet at $\delta = 7.85$ ppm and a multiplet around $\delta = 7.0$ ppm for the *trans*-azoBTA model compound. Upon photoisomerisation the doublet disappears while the multiplet shifts downfield to $\delta \approx 6.8$ ppm, which is indicative for the presence of the *cis* isomer. As expected, no signal is visible in the spectrum for azoBTA in d_{14}-MCH at room temperature before irradiation—apart from the reference $CHCl_3$ at $\delta =$ 7.26—since the majority of the azoBTA is assembled (Figure 4C). Signals appear in d_{14}-MCH at $T = 75\,^\circ$C before irradiation (Figure 4D, $\delta = 7.97$, 7.12 and 7.01 ppm), and at room temperature after irradiation with UV light (Figure 4E, respectively). Before irradiation the chemical shifts of the peaks correspond well with the *trans* isomer of the model compound, and the appearance of peaks after UV irradiation indicates that the fibres have (partially) depolymerised.

We now turn to UV-vis spectroscopy to study the photoisomerisation in more detail and attempt to obtain control over the fraction of isomerised azoBTA by stepwise irradiation. Stepwise irradiation (steps of 1 s separated by 59 s intervals for spectral acquisition and sample handling) facilitates the investigation of the isomerisation and dissociation states that lie between the predominantly *trans* pristine state, and the predominantly *cis* state obtained after irradiation at $\lambda = 365$ nm. A typical UV-vis absorption spectrum of pristine, non-associated, predominantly *trans*-azoBTA in chloroform is depicted in Figure 5A in blue. It shows a strong $\pi \rightarrow \pi^*$ absorption around $\lambda =$ 365 nm and a weak $n \rightarrow \pi^*$ absorption around $\lambda = 420$ nm, both originating from *trans*-azobenzene. Upon stepwise irradiation with λ_{365nm} the peak originating from the $\pi \rightarrow \pi^*$ transition gradually decreases in intensity, and a weak absorption centred at $\lambda = 445$ nm appears for the $n \rightarrow \pi^*$ transition of the *cis* isomer. Within 29 steps of 1 s irradiation we reach a characteristic spectrum for predominantly *cis*-azobenzene that hardly changes upon continued irradiation. Subsequent exposure to stepwise irradiation at $\lambda = 455$ nm induces the reverse process: the absorption band at $\lambda = 365$ nm increases in intensity, while simultaneously the $n \rightarrow \pi^*$ band undergoes a hypsochromic shift from $\lambda = 455$ nm to 420 nm (Figure 5B). After 34 steps of 1 s irradiation, the absorption spectrum appears constant with continued irradiation.

Surprisingly, the intensity of the absorption maximum at $\lambda =$ 365 nm after a more-than-equivalent number of backward irradiation steps with λ_{455nm} is approximately 20% below its initial value. Therefore, we investigate the thermal relaxation of the azoBTA-CO_2Et model compound through ^{1}H NMR. We determine the percentage *trans*-azobenzenes as a function of relaxation time from the ratio of peak integrals at characteristic chemical shifts for the *trans* and *cis* isomers—specifically the ratio between peaks at $\delta = 7.85$ and 8.35. Herewith we determine the half-life of the *cis* isomer in $CDCl_3$ to be about 24 h. From these kinetics we find that the thermal recovery of the last 20% or so of *cis*-azobenzene still present after 30×1 s irradiation steps at λ_{455nm} will take approximately 100 h at room

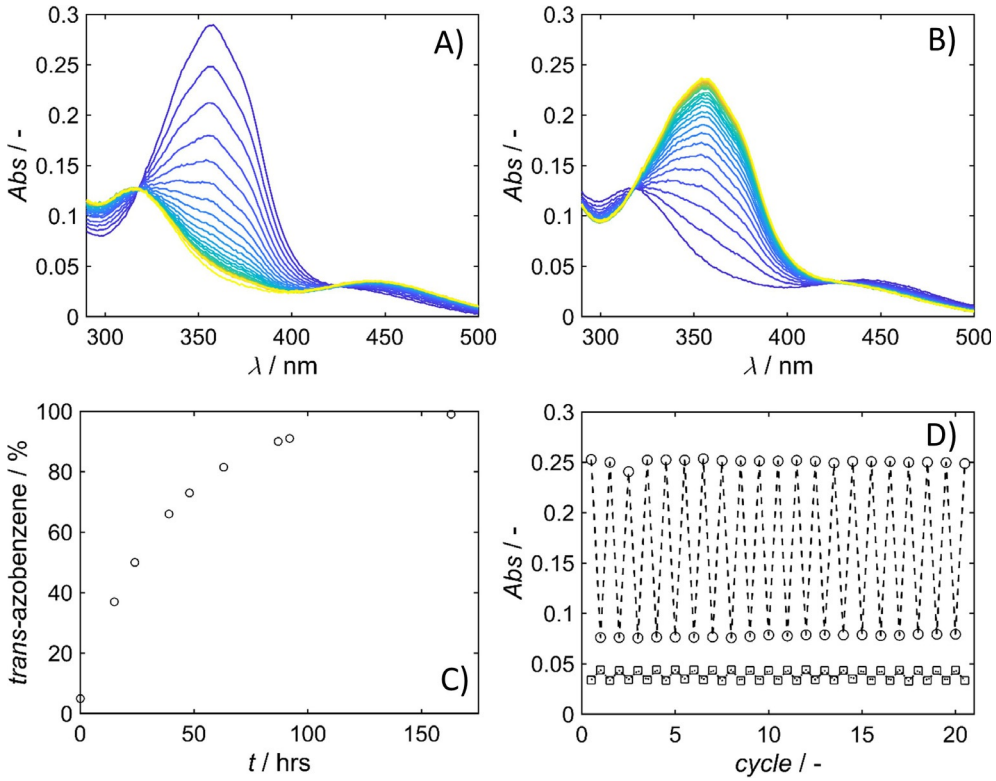

Figure 5. (Photo-)isomerisation of non-associated azoBTA. A) UV-vis spectra of stepwise *trans* (blue) to *cis* (yellow) photoisomerisation through irradiation at λ_{365nm}, and B) the reverse *cis* (blue) to *trans* (yellow) is achieved by irradiation at λ_{455nm}. Irradiation experiments in A and B are performed at 15 μM in $CHCl_3$ at room temperature with small doses of weak-intensity light corresponding to 1 s at 10% of the LED intensity at 1000 mA. C) Thermal *cis*-to-*trans* relaxation of 300 μM azoBTA-CO_2Et in $CDCl_3$ at room temperature as monitored by ^{1}H NMR spectroscopy. The monomers were isomerised to *cis* by 15 min irradiation with high intensity UV light at 600 mA. D) The photoisomerisation of azoBTA is reversible for at least 20 cycles as shown by UV-vis absorption values at A_{365nm} for the *trans*-azoBTA (circles) and A_{455nm} for *cis*-azoBTA (squares). The 15 μM solution in chloroform was irradiated at room temperature for 10 s at 100% of the LED intensity at 1000 mA.

temperature; equivalent to the recovery from 80% to approximately 100% *trans*-azobenzene in Figure 5C. This strongly suggests that it is possible to isomerise the remaining fraction of *cis*-isomers (Figure 5C), additionally considering that *trans*-azoBTA is the most favourable conformation (Figure S22, S23).

Having established that the photoisomerisation is fully reversible, though slow, we evaluate the robustness of the process. To this end a 15 μM azoBTA solution is alternatingly illuminated with 365 nm and 455 nm light for 10 s (Figure 5D). Gratifyingly, we observe little to no difference in the maximum A_{365nm} and A_{455nm} between 20 successive cycles as we repeatedly switch between *trans*- and *cis*-azoBTA.

Fibre dissociation through irradiation

Now that we have confirmed that the azobenzenes are light-responsive in the assembled azoBTA molecules, we investigate the effect of the photoisomerization on the assembly state in more detail through UV-vis and CD spectroscopy. We perform stepwise irradiation experiments in MCH at room temperature and observe the changes in UV-vis and CD spectra. Upon stepwise irradiation at λ_{365nm}, we again observe a gradual decrease of the intensity of the *trans*-$\pi\rightarrow\pi^*$ absorption peak around 365 nm, and the simultaneous increase in intensity of A_{455nm} (Figure 6A). The consecutive spectra recorded for λ_{365nm} irradiation in MCH are spaced closer together than the equivalent spectra recorded for azoBTA in chloroform (Figure 5A), and a longer total irradiation time is needed to reach a state where the spectrum barely changes with continued irradiation. These combined observations indicate that in MCH a higher energy barrier for isomerisation exists, which we attribute to the strong attractions and close packing of the molecules in the fibres. Irradiation at λ_{455nm} recovers the *trans* isomer to a large extent. The shape of the obtained UV-vis absorption spectrum after *trans-cis-trans* photoisomerisation has features of both *trans*-azoBTA in $CHCl_3$ and of the initial spectrum in MCH (Figure S24), which indicates that the azobenzenes are less or differently organised than before irradiation.

We exploit the inclusion of the two γ-(S) stereogenic centres per azoBTA monomer to monitor the presence of excess right- or left-handed superstructures by CD spectroscopy. We find that the *trans*-to-*cis* isomerisation upon stepwise irradiation with λ_{365nm} (Figure 6A) is accompanied by a complete loss of the azobenzene CD signal, while the Cotton effect of the BTA is merely reduced in intensity (Figure 6B). This implies that the photoisomerisation to *cis*-azoBTA triggers the disappearance of the helical azobenzene superstructure, while the BTA core of the fibres dissociates but does not disintegrate entirely.

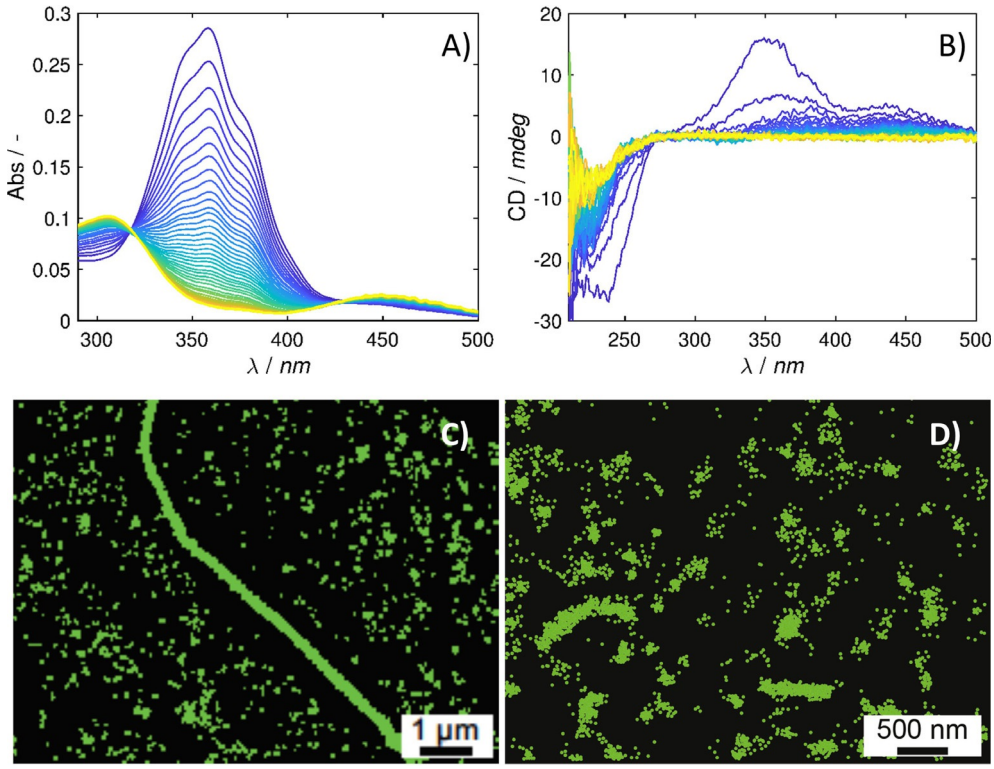

Figure 6. Depolymerization of azoBTA fibres by UV irradiation. A) UV-vis absorption and B) CD spectra of the stepwise irradiation of a 15 μM azoBTA solution in MCH at room temperature with small doses corresponding to 1 s at 10% of the LED intensity at 1000 mA of λ_{365nm} shows the *trans* (blue) to *cis* (yellow) photoisomerisation of the azobenzene in the azoBTA fibres. Super-resolved iPAINT reconstructions before C) and after D) irradiation of a 300 μM azoBTA solution with λ_{365nm} (1 s at 50% of the LED intensity at 1000 mA) show that the large fibrillar structures disappear upon exposure to UV light.

We employ iPAINT super-resolution microscopy[23] to visualise the fibres and confirm that the disappearance of the CD signal upon UV irradiation is not explained by for example, helix inversion. Therefore, we study a 300 μM sample before and after a brief irradiation (1 s) at $\lambda = 365$ nm, which should result in partial depolymerisation. Before irradiation we observe fibres of several microns long with a high polydispersity in length (Figure 6C and Figure S25), while we find only sub-micron sized fragments after 1 s of irradiation (Figure 6D and Figure S25). Although the details of the fragmentation process have not been elucidated, these results once more suggest that we actively disrupt the fibres by photoisomerising azobenzenes in the assembled state.

Conclusions

Azobenzene-substituted BTA monomers in MCH spontaneously form hydrogen-bonded supramolecular fibres in MCH below $T \approx 75\,^{\circ}C$, as shown by FTIR, iPAINT, and CD and UV-vis spectroscopy. The stability of the hydrogen bonded network between BTA cores is also confirmed by MD simulations. The azoBTAs form a 1D helical assembly wherein the helicity of the BTA cores is opposite to the double helix formed by the azobenzene substituents. Additionally, the azobenzenes remain addressable with UV irradiation at a wavelength of $\lambda = 365$ nm when the azoBTA is assembled into fibres, and the UV-induced *trans*-to-*cis* isomerisation depolymerises the supramolecular fibres. The formation of a discordant helical nanoarchitecture appears robust; it is regenerated after thermal depolymerisation, after *cis-trans* photoisomerisation, and after thermal relaxation. This work demonstrates that a single photoswitch per monomer suffices to depolymerise a supramolecular BTA construct.

Experimental Section

Synthesis and characterisation of methyl-(*E*)-4-(4-((4-(2-((tert-butoxycarbonyl)amino)ethoxy)phenyl)diazenyl)phenoxy)butanoate (1): (*E*)-4,4′-(diazene-1,2-diyl)diphenol (2.51 g, 11.67 mmol), *tert*-butyl (2-bromoethyl)carbamate (1.72 g, 7.67 mmol), methyl 4-bromobutanoate (3.17 g, 17.51 mmol), potassium carbonate (8.08 g, 134.7 mmol) and sodium iodide (187 mg, 1.25 mmol) were suspended in DMF (55 mL) by sonication. The reaction mixture was stirred at 100 °C for 24 hours under argon. The mixture was poured into 500 mL water (pH 6), the precipitate was collected by filtration and washed with acidic water (pH 6). The crude product was dried in a vacuum oven, and subsequently purified by column chromatography (SiO_2, CH_2Cl_2:EtOAc from 20% to 40% EtOAc in 15 column volumes) to yield compound 1 (yellow powder, 1.55 g, 49% yield). ^{1}H NMR (400 MHz, $CDCl_3$, 97:3 *E*/*Z* mixture, signals of the main isomer) δ: 7.86 (d, $J = 8$ Hz, 4H), 6.99 (d, $J = 8$ Hz, 4H), 5.00 (t, $J = 8$ Hz, 1H), 4.09 (q, $J = 8$ Hz, 2H), 3.71 (s, 3H), 3.58 (m, 2H), 2.56 (t, $J = 8$ Hz, 2H), 2.15 (p, $J = 8$ Hz, 2H), 1.46 (s, 9H). ^{13}C NMR (100 MHz, $CDCl_3$) δ: 174.02, 161.09, 147.08, 124.58, 124.55, 114.84, 67.14, 51.95, 30.69, 28.51, 24.72. UV-vis ($CHCl_3$): $\varepsilon_{358.5} = 6.77 \times 10^4$ cm^{-1} M^{-1}. FT-IR (ATR) ν (cm^{-1}): 3281, 3060, 3004, 2979,

2969, 2930, 2061, 1985, 1908, 1735, 1719, 1687, 1595, 1542, 1496, 1460, 1439, 1386, 1361, 1329, 1302, 1275, 1249, 1207, 1176, 1144, 1107, 1064, 1048, 1039, 1017, 997, 939, 883, 869, 812, 779, 732, 695, 640, 585, 566, 556, 533, 518, 484, 464. MALDI-ToF-MS (*m/z*): [M^+] calcd for $C_{24}H_{31}N_3O_6$ 457.22; found 457.25.

Synthesis and characterisation of methyl 4-(4-((*E*)-(4-(2-(3,5-bis(((*S*)-3,7-dimethyloctyl)carbamoyl)benzamido)ethoxy)phenyl)-diazenyl)phenoxy)butanoate (2): 3,5-bis(((*S*)-3,7-dimethyloctyl)carbamoyl)benzoic acid (400 mg, 0.82 mmol) was synthesised via a previously reported protocol,[24] and was suspended in dry DCM (15 mL) under argon. Ghosez's reagent (164 mg, 1.23 mmol) was added. The suspension was stirred for 3 hours and eventually became a clear solution. The volatiles were removed under vacuum. Compound **1** (374 mg, 0.82 mmol) was dissolved in 5% TFA in chloroform. After 3 hours of stirring, the volatiles were removed under vacuum. The dried residue was redissolved in chloroform (20 mL) and triethylamine (331 mg, 3.27 mmol) was added. This mixture was stirred at RT for 10 minutes and subsequently added dropwise to a solution of the acyl chloride residue in chloroform (10 mL) at 0 °C. After the addition, the reaction was allowed to proceed at room temperature for 12 hours under argon. The solvent was removed and the crude product purified by column chromatography (SiO_2, Reveleris 120 g, $CHCl_3$:EtOAc from 20% to 40% EtOAc in 10 column volumes) to obtain compound 2 (yellow powder, 0.51 g, 75% yield). ^{1}H NMR (400 MHz, $CDCl_3$, 94:6 *E/Z* mixture, signals of the main isomer) δ: 8.35 (d, J=4 Hz, 2H), 8.33 (t, J=4 Hz, 1H), 7.86 (d, J=4 Hz, 4H), 7.01–6.96 (m, 5H), 6.43 (t, J=8 Hz, 2H), 4.22 (t, J=8 Hz, 2H), 4.08 (t, J=8 Hz, 2H), 3.93 (q, J=8 Hz, 2H), 3.70 (s, 3H), 3.51–3.44 (m, 4H), 2.55 (t, J=8 Hz, 2H), 2.15 (p, J=8 Hz, 2H), 1.65–1.09 (m, 20H), 0.93 (d, J=8 Hz, 6H), 0.85 (d, J=8 Hz, 12H). ^{13}C NMR (100 MHz, $CDCl_3$) δ: 173.71, 166.15, 165.69, 161.04, 160.38, 147.53, 147.17, 135.56, 134.95, 128.33, 128.17, 124.55, 124.53, 114.83, 114.79, 67.12, 66.87, 53.57, 51.83, 39.92, 39.38, 38.69, 37.26, 36.77, 30.90, 30.63, 28.09, 24.77, 24.72, 22.84, 22.74, 19.63. UV-vis ($CHCl_3$): $\varepsilon_{357}=3.16\times10^4$ cm^{-1} M^{-1}. FT-IR (ATR) ν (cm^{-1}): 3238, 3071, 2953, 2926, 2870, 1739, 1638, 1599, 1559, 1500, 1467, 1437, 1381, 1366, 1299, 1247, 1172, 1149, 1107, 1056, 1005, 943, 905, 885, 841, 805, 731, 692, 589, 551. MALDI-ToF-MS (*m/z*): [$M+Na^+$] calcd for $C_{49}H_{71}N_5O_7$ 841.54; found 864.53.

Synthesis and characterisation of 4-(4-((*E*)-(4-(2-(3,5-bis(((*S*)-3,7-dimethyloctyl)carbamoyl)benzamido)ethoxy)phenyl)diazenyl)-phenoxy)butanoic acid (3): Compound **2** (480 mg, 0.58 mmol) was dissolved in 1,2-dichloroethane (10 mL), and trimethylstannanol (6.12 mg, 3.38 mmol) was added. The mixture was stirred at 70 °C for 24 hours. The solvent was removed and the crude product dried in a vacuum oven. The dried crude was loaded on a paper filter and washed copiously with water to remove Sn by-products. The obtained product (463 mg, 0.57 mmol, 98% yield) was dried overnight in a vacuum oven. ^{1}H NMR (400 MHz, $CDCl_3$) δ: 8.36 (d, J=4 Hz, 2H), 8.34 (t, J=4 Hz, 1H), 7.85 (d, J=8 Hz, 4H), 7.02–6.97 (m, 5H), 6.39 (t, J=8 Hz, 2H), 4.23 (t, J=8 Hz, 2H), 4.08 (t, J=8 Hz, 2H), 3.93 (q, J=8 Hz, 2H), 3.55–3.41 (m, 4H), 2.52 (t, J=8 Hz, 2H), 2.12 (p, J=8 Hz, 2H), 1.57–1.10 (m, 20H), 0.94 (d, J=8 Hz, 6H), 0.86 (d, J=8 Hz, 12H). ^{13}C NMR (100 MHz, $CDCl_3$) δ: 178.61, 166.11, 165.64, 161.27, 160.34, 147.57, 147.08, 135.55, 134.94, 128.33, 128.17, 124.53, 124.51, 114.85, 114.83, 67.52, 66.90, 53.57, 39.93, 39.39, 38.69, 37.27, 36.78, 31.30, 30.90, 28.10, 25.47, 24.77, 22.85, 22.74, 19.64. UV-vis (DMSO): $\varepsilon_{364}=1.58\times10^4$ cm^{-1} M^{-1}. FT-IR (ATR) ν (cm^{-1}): 3244, 3072, 2954, 2926, 2869, 1641, 1596, 1562, 1500, 1468, 1383, 1297, 1248, 1198, 1148, 1106, 1052, 908, 841, 773, 731, 692, 548. MALDI-ToF-MS (*m/z*): [$M+Na^+$] calcd for $C_{47}H_{67}N_5O_7$ 814.08; found 836.49.

Synthesis and characterisation of 3,4,5-tris(dodecyloxy)benzyl4-(4-((*E*)-(4-(2-(3,5-bis(((*S*)-3,7-dimethyloctyl)carbamoyl)benzamido)ethoxy)phenyl)diazenyl)phenoxy)butanoate (azoBTA): Compound **3** (160 mg, 0.2 mmol) was dissolved in dry DCM (15 mL) under argon, then Ghosez reagent (40 mg, 0.30 mmol) was added. The solution was stirred for 3 hours and the volatiles were removed under vacuum. The crude material was redissolved in dry DCM (10 mL) and the solution cooled down to 0 °C (ice bath). Triethylamine (80 μL, 0.59 mmol) was added, followed by a dropwise addition (syringe, 5 minutes) of 3,4,5-tris(dodecyloxy)benzyl alcohol (131 mg, 0.2 mmol) dissolved in dry DCM (5 mL). The solution was stirred for 10 minutes at 0 °C, and then at room temperature for 12 hours. The solvent was removed and the crude product purified by column chromatography (SiO_2, Reveleris Silica 80 g, $CHCl_3$:EtOAc from 0% to 40% EtOAc in 15 column volumes) to obtain compound 4 (yellow powder, 60 mg, 20% yield). ^{1}H NMR (400 MHz, $CDCl_3$, 88:12 *E/Z* mixture, signals of the main isomer) δ: 8.35 (d, J=4 Hz, 2H), 8.33 (t, J=4 Hz, 1H), 7.85 (d, J=8 Hz, 4H), 7.15 (t, J=8 Hz, 1H), 6.98 (dd, J_1=8 Hz, J_2=12 Hz, 4H), 6.57 (t, J=8 Hz, 2H), 6.54 (s, 2H), 5.03 (s, 2H), 4.21 (t, J=8 Hz, 2H), 4.08 (t, J=8 Hz, 2H), 3.96–3.90 (m, 8H), 3.50–3.43 (m, 4H), 2.60 (t, J=8 Hz, 2H), 2.16 (p, J=8 Hz, 2H), 1.81–1.40 (m, 20H), 1.30–1.26 (m, 56H), 1.14 (t, J=8 Hz, 6H), 0.92 (d, J=8 Hz, 6H), 0.87 (t, J=8 Hz, 9H), 0.86 (d, J=8 Hz, 12H). ^{13}C NMR (100 MHz, $CDCl_3$) δ: 173.09, 166.27, 165.80, 160.98, 160.38, 153.34, 147.48, 147.14, 138.35, 135.54, 134.93, 130.84, 128.35, 128.20, 124.53, 124.51, 114.79, 114.73, 107.12, 73.55, 69.26, 67.09, 66.93, 66.82, 39.90, 39.36, 38.68, 37.25, 36.74, 32.07, 32.06, 30.93, 30.89, 30.47, 29.88, 29.87, 29.83, 29.79, 29.78, 29.75, 29.56, 29.53, 29.50, 28.06, 26.26, 26.24, 24.75, 22.82, 22.72, 19.60, 14.25. UV-vis ($CHCl_3$): $\varepsilon_{358.5}=2.61\times10^4$ cm^{-1} M^{-1}. FT-IR ν (cm^{-1}): 3239, 3072, 2922, 2853, 1735, 1638, 1596, 1558, 1501, 1467, 1439, 1380, 1332, 1299, 1245, 1149, 1115, 1057, 948, 904, 841, 721, 692, 550. MALDI-ToF-MS (*m/z*): [$M+Na^+$] calcd for $C_{90}H_{145}N_5O_{10}$ 1457.17; found 1480.10.

Commercial chemicals were obtained from TCI and/or Sigma Aldrich. Used as received without further purification. Methylcyclohexane was dried over mol sieves and degassed by bubbling N_2 before use.

CD and UV-vis: spectra were recorded simultaneously on a Jasco J815 CD spectrometer, equipped with a PTC-423 s/5 Peltier cell holder. Measuring parameters were chosen appropriately. A sealable quartz cell was used. The spectra in Figure 2A, C, S17 were recorded in continuous mode between 550–190 nm at every 2 nm, with a sensitivity of 100 mdeg, at 100 nm min^{-1}. The integration time was set to 0.25 s. The temperature was changed at 10 °C h^{-1}. The spectra in Figure 6A and B were recorded simultaneously and in continuous mode between 550–190 nm at every 0.5 nm, with a sensitivity of 100 mdeg, at 1000 nm min^{-1}.The response time was set to 0.125 s, and spectra were recorded at an interval of 1 min. The spectra in Figure S22 were recorded continuously between 450–350 nm and 270–200 nm at every 0.5 nm, with a sensitivity of 100 mdeg, at 200 nm min^{-1}. The response time was set to 0.5 s, and spectra were recorded at an interval of 1 min. The spectra in Figure S23 were recorded continuously between 550–200 nm at every 0.5 nm, with a sensitivity of 100 mdeg, at 500 nm min^{-1}. The response time was set to 0.5 s, and spectra were recorded at an interval of 5 min for the first 5 h, after which manually another series was started at an interval of 10 min.

UV-vis: spectra (Figure 5) were recorded on a Shimadzu 2700 UV-visible spectrophotometer. Spectra were recorded between 500–290 nm with 1 nm sampling. The wavelength was continuously changed 'fast' during the recording of a spectrum, and spectra were recorded at an interval of 60 s. The light source was changed

at 310 nm. A sealable quartz cell with a path length of 1 cm was used. The temperature was held constant at 20 °C.

IR: spectra were recorded on a PerkinElmer Spectrum One 1600 FT-IR spectrometer or a PerkinElmer Spectrum Two FT-IR spectrometer, equipped with a PerkinElmer Universal ATR Sampler Accessory. FT-IR spectra in liquid were recorded in a sealed cell with CaF_2 windows.

^{1}H NMR and ^{13}C NMR: spectra were recorded either on a Varian Mercury Vx 400 MHz (100 MHz for ^{13}C) or Varian Oxford AS 500 MHz (125 MHz for ^{13}C) NMR spectrometers. Chemical shifts are given in ppm (δ) values relative to residual solvent or tetramethylsilane (TMS). Splitting patterns are labelled as s, singlet; d, doublet; t, triplet; q, quartet; p, pentet; m, multiplet.

MALDI-ToF-MS: (Matrix assisted laser desorption/ionisation time of flight mass spectroscopy) was performed on a PerSeptive Biosystems Voyager DE-PRO spectrometer or a Bruker autoflex speed spectrometer using α-cyano-4-hydroxycinnamic acid (CHCA) and 2-[(2E)-3-(4-tert-butylphenyl)-2-methylprop-2-enylidene]malononitrile (DCTB) as matrices.

Karl–Fisher: titrations were carried out on a Mettler-Toledo C30 Coulometric KF titrator containing CombiCoulomat Frit KF reagent. Samples of approximately 0.5 mL were injected directly into the medium, and averages of at least 2 measurements were taken as the water content.

SAXS: (Small-angle X-ray scattering) measurements were performed on a Saxslab Ganesha vacuum system with a Pilatus 300k solid-state photon-counting 2D-detector and a high brilliance Microfocus Cu radiation source, Genix3D, wavelength $\lambda = 1.54184$ Å. Measurements were obtained in transmission mode using a sample-to-detector distance of 80 mm for WAXS and up to 1400 mm for SAXS. A silver behenate standard was used to calibrate the *q*-scale. The samples were prepared in 2 mm quartz glass capillaries. Fitting of the data with a core–shell cylinder model,[19] with a scattering length density of $3.8 \pm 0.02 \times 10^{-6}$ Å^{-2} for the core, 1.2 ± 0.01 02×10^{-6} Å^{-2} for the shell and 1.1 ± 0.01 02×10^{-6} Å^{-2} for the solvent, yields a radius of 13.8 Å for the core and a shell thickness of 19.0 Å. The cylinder length *L* is longer than the attainable resolution of the instrument.

Super-resolution microscopy: A recently reported protocol[23] for iPAINT imaging[25] is modified and used to image the adsorbed supramolecular fibres in DMSO.[26] Briefly, a 300 μM solution of azoBTA in MCH was flushed into the imaging cell and dried under a gentle stream of nitrogen. The dried sample was stained by flushing 0.5% v/v of Cage-552 (10 mM in DMSO) and 1% v/v of *i*PrOH in MCH into the imaging cell. iPAINT images were acquired on an inverted *N*-Storm Nikon microscope equipped with a $\lambda =$ 561 nm laser ($\approx$490 mW cm^{-2}), and a $\lambda = 405$ nm laser ($\approx$160 mW cm^{-2}). The incident light passes through a quad-band pass dichroic mirror (95335 Nikon) and is focused on the sample with a Nikon objective (oil immersion, 100×, NA = 1.49). The sample illumination occurs in a quasi-Total Internal Reflection Fluorescence (TIRF) geometry. iPAINT images were taken on 256×256 pixels region of interest at an acquisition frame rate of 47 fps on an EMCCD Ixon3 Andor camera (pixel size 17×17 μm). Photons are collected over 5×10^3 frames during which 0.5% of the UV laser line is illuminating the sample continuously, along with 100% power of the 561 nm laser. The UV laser is used to stochastically uncage a small amount of the caged (dark, non-fluorescent) probes warranting a spatial separation greater than the diffraction limit of light. UV irradiation turns the dark probes into an open (bright, fluorescent) conformational state of which the absorption maximum falls in the visible region of the spectrum, enabling excitation and bleaching by the 561 nm laser. The localisation of single molecules is carried out by NIS-element Nikon software. The super-resolved iPAINT images were corrected for background localisations using a density-based algorithm. The point-cloud of localisations is screened for all data points with *n* neighbours within a certain area of radius δ. With the iPAINT images being a 2D projection of 3D localisations, the density of single molecules identified along the fibres is higher than those localised on the coverslip, granting a straightforward identification of the supramolecular structures.

Sample preparation: For UV-vis and CD spectroscopy (15 μM), solution-IR spectroscopy (0.5 mM), SAXS (3 mM), and iPAINT and ^{1}H NMR (0.3 mM) analysis, azoBTA (**4**) or the model compound azoBTA-CO_2Et (**5**, Figure S21) was dissolved at target concentration in dried MCH at 75 °C, or in $CHCl_3$ at room temperature, and allowed to equilibrate at rt for at least 24 h before measurements.

Molecular Dynamics simulations: *Modelling and simulation procedures*: The atomistic model of the azoBTA monomer has been parametrised in the framework of GAFF (General Amber Force Field).[20] The force field parameters for the BTA core and alkyl groups have been taken from previous simulation works on BTA supramolecular polymers.[11b,21] The force field parameters for the additional *trans* azobenzene unit in the azoBTA has been taken from other previous works.[7,27] The molecular models for the azoBTA stacks (Figure 3 a in the main paper) have been then inserted into simulation boxes filled with explicit MCH molecules. The simulation boxes were built in such a way to effectively model a portion of the bulk of infinite supramolecular polymers via periodic boundary conditions (PBC). The all atom molecular dynamics (AA-MD) simulations were performed with the GROMACS software (2016 version).[28] After an initial minimization, all AA-MD runs have been conducted in NPT conditions (constant N: number of particles, P: pressure and T: temperature) at 300 K (using the v-rescale thermostat[29] with a coupling constant of 1 ps) and 1 atm (using semi-isotropic pressure scaling to allow the fibres to fold) with a coupling constant of 1 ps. The Particle Mesh Ewald (PME)[30] method was used to treat long-range electrostatics. The LINCS algorithm was used to constrain all bonds involving hydrogens.[31] For what concerns the analysis of the AA-MD simulation results, we used GROMACS built-in analysis tools: *gmx energy* for energetic analysis and *gmx rdf* for the calculation of radial distribution functions.

Acknowledgements

The authors acknowledge the Netherlands Organisation for Scientific Research (NWO VIDI Grant 723.014.006) and the Dutch Ministry of Education, Culture and Science (Gravity Program 024.001.035) for financial support. The ICMS Animation Studio (Eindhoven University of Technology) is acknowledged for providing the artwork for Figure 1. GMP acknowledges the funding received by the Swiss National Science Foundation (SNSF grant number 200021 175735) and by the European Research Council (ERC) under the European Union's Horizon 2020 research and innovation programme (grant agreement no. 818776–DYNAPOL). M.M.R.M. Hendrix is acknowledged for performing the SAXS measurements, and A. Aloi for performing the iPAINT imaging.

Conflict of interest

The authors declare no conflict of interest.

Keywords: benzene-1,3,5-tricarboxamide · photoisomerisation · photoswitch · responsive · supramolecular polymer

[1] a) S. Cantekin, T. F. A. de Greef, A. R. A. Palmans, *Chem. Soc. Rev.* **2012**, *41*, 6125 – 6137; b) S. Yagai, K. Ohta, M. Gushiken, K. Iwai, A. Asano, S. Seki, Y. Kikkawa, M. Morimoto, A. Kitamura, T. Karatsu, *Chem. Eur. J.* **2012**, *18*, 2244 – 2253.

[2] a) B. Adhikari, Y. Yamada, M. Yamauchi, K. Wakita, X. Lin, K. Aratsu, T. Ohba, T. Karatsu, M. J. Hollamby, N. Shimizu, H. Takagi, R. Haruki, S.-I. Adachi, S. Yagai, *Nat. Commun.* **2017**, *8*, 15254; b) E. Fuentes, M. Gerth, J. A. Berrocal, C. Matera, P. Gorostiza, I. K. Voets, S. Pujals, L. Albertazzi, *J. Am. Chem. Soc.* **2020**, *142*, 10069 – 10078; c) K. K. Kartha, N. K. Allampally, A. T. Politi, D. D. Prabhu, H. Ouchi, R. Q. Albuquerque, S. Yagai, G. Fernández, *Chem. Sci.* **2019**, *10*, 752 – 760.

[3] a) R. Klajn, P. J. Wesson, K. J. M. Bishop, B. A. Grzybowski, *Angew. Chem. Int. Ed.* **2009**, *48*, 7035 – 7039; *Angew. Chem.* **2009**, *121*, 7169 – 7173; b) S. Lee, S. Oh, J. Lee, Y. Malpani, Y.-S. Jung, B. Kang, J. Y. Lee, K. Ozasa, T. Isoshima, S. Y. Lee, M. Hara, D. Hashizume, J.-M. Kim, *Langmuir* **2013**, *29*, 5869 – 5877; c) O. M. Wani, R. Verpaalen, H. Zeng, A. Priimagi, A. P. H. J. Schenning, *Adv. Mater.* **2019**, *31*, 1805985 – 1805985.

[4] S. S. D. Lafleur, L. Shen, E. J. T. W. Kamphuis, S. J. A. Houben, L. Balzano, J. R. Severn, A. P. H. J. Schenning, C. W. M. Bastiaansen, *Macromol. Rapid Commun.* **2019**, *40*, 1800811 – 1800811.

[5] J. Kim, J. Lee, W. Y. Kim, H. Kim, S. Lee, H. C. Lee, Y. S. Lee, M. Seo, S. Y. Kim, *Nat. Commun.* **2015**, *6*, 6959.

[6] C. Maity, W. E. Hendriksen, J. H. Van Esch, R. Eelkema, *Angew. Chem. Int. Ed.* **2015**, *54*, 998 – 1001; *Angew. Chem.* **2015**, *127*, 1012 – 1015.

[7] J. W. Fredy, A. Méndez-Ardoy, S. Kwangmettatam, D. Bochicchio, B. Matt, M. C. A. Stuart, J. Huskens, N. Katsonis, G. M. Pavan, T. Kudernac, *Proc. Natl. Acad. Sci. USA* **2017**, *114*, 11850 – 11855.

[8] J. Lee, S. Oh, J. Pyo, J.-M. Kim, J. H. Je, *Nanoscale* **2015**, *7*, 6457 – 6461.

[9] a) A. A. Beharry, O. Sadovski, G. A. Woolley, *J. Am. Chem. Soc.* **2011**, *133*, 19684 – 19687; b) D. Bléger, J. Schwarz, A. M. Brouwer, S. Hecht, *J. Am. Chem. Soc.* **2012**, *134*, 20597 – 20600; c) D. Manna, T. Udayabhaskararao, H. Zhao, R. Klajn, *Angew. Chem. Int. Ed.* **2015**, *54*, 12394 – 12397; *Angew. Chem.* **2015**, *127*, 12571 – 12574.

[10] a) R. P. M. Lafleur, X. Lou, G. M. Pavan, A. R. A. Palmans, E. W. Meijer, *Chem. Sci.* **2018**, *9*, pp. 6199 – 6209; b) Y. Nakano, T. Hirose, P. J. M. Stals, E. W. Meijer, A. R. A. Palmans, *Chem. Sci.* **2012**, *3*, pp. 148 – 155.

[11] a) D. Bochicchio, G. M. Pavan, *ACS Nano* **2017**, *11*, 1000 – 1011; b) M. Garzoni, M. B. Baker, C. M. A. Leenders, I. K. Voets, L. Albertazzi, A. R. A. Palmans, E. W. Meijer, G. M. Pavan, *J. Am. Chem. Soc.* **2016**, *138*, 13985 – 13995; c) A. J. Markvoort, H. M. M. ten Eikelder, P. A. J. Hilbers, T. F. A. de Greef, E. W. Meijer, *Nat. Commun.* **2011**, *2*, 509.

[12] a) L. Albertazzi, N. van der Veeken, M. B. Baker, A. R. A. Palmans, E. W. Meijer, *Chem. Commun.* **2015**, *51*, 16166 – 16168; b) C. M. A. Leenders, L. Albertazzi, T. Mes, M. M. E. Koenigs, A. R. A. Palmans, E. W. Meijer, *Chem. Commun.* **2013**, *49*, 1963 – 1965.

[13] a) M. A. J. Gillissen, T. T. Hoeben, A. J. H. Spiering, J. A. J. M. Vekemans, A. R. A. Palmans, E. W. Meijer, *Isr. J. Chem.* **2011**, *51*, 1118 – 1127; b) T. Mes, M. M. J. Smulders, A. R. A. Palmans, E. W. Meijer, *Macromolecules* **2010**, *43*, 1981 – 1991.

[14] K. Kreger, P. Wolfer, H. Audorff, L. Kador, N. Stingelin-Stutzmann, P. Smith, H.-W. Schmidt, *J. Am. Chem. Soc.* **2010**, *132*, 509 – 516.

[15] M. M. J. Smulders, A. P. H. J. Schenning, E. W. Meijer, *J. Am. Chem. Soc.* **2008**, *130*, 606 – 611.

[16] M. M. J. Smulders, T. Buffeteau, D. Cavagnat, M. Wolffs, A. P. H. J. Schenning, E. W. Meijer, *Chirality* **2008**, *20*, 1016 – 1022.

[17] M. Masuda, P. Jonkheijm, R. P. Sijbesma, E. W. Meijer, *J. Am. Chem. Soc.* **2003**, *125*, 15935 – 15940.

[18] S. Yagai, Y. Goto, X. Lin, T. Karatsu, A. Kitamura, D. Kuzuhara, H. Yamada, Y. Kikkawa, A. Saeki, S. Seki, *Angew. Chem. Int. Ed.* **2012**, *51*, 6643 – 6647; *Angew. Chem.* **2012**, *124*, 6747 – 6751.

[19] S. Kline, R. Heenan, **2013**, http://www.sasview.org/sasmodels/model/core_shell_cylinder.html.

[20] J. Wang, R. M. Wolf, J. W. Caldwell, P. A. Kollman, D. A. Case, *J. Comput. Chem.* **2004**, *25*, 1157 – 1174.

[21] M. B. Baker, L. Albertazzi, I. K. Voets, C. M. A. Leenders, A. R. A. Palmans, G. M. Pavan, E. W. Meijer, *Nat. Commun.* **2015**, *6*, 6234.

[22] D. Bochicchio, S. Kwangmettatam, T. Kudernac, G. M. Pavan, *ACS Nano* **2019**, *13*, 4322 – 4334.

[23] B. Adelizzi, A. Aloi, N. J. Van Zee, A. R. A. Palmans, E. W. Meijer, I. K. Voets, *ACS Nano* **2018**, *12*, 4431 – 4439.

[24] M. L. Ślęczkowski, E. W. Meijer, A. R. A. Palmans, *Macromol. Rapid Commun.* **2017**, *38*, 1700566.

[25] A. Aloi, N. Vilanova, L. Albertazzi, I. K. Voets, *Nanoscale* **2016**, *8*, 8712 – 8716.

[26] A. Aloi, A. Vargas Jentzsch, N. Vilanova, L. Albertazzi, E. W. Meijer, I. K. Voets, *J. Am. Chem. Soc.* **2016**, *138*, 2953 – 2956.

[27] L. Pesce, C. Perego, A. B. Grommet, R. Klajn, G. M. Pavan, *J. Am. Chem. Soc.* **2020**, *142*, 9792 – 9802.

[28] M. J. Abraham, T. Murtola, R. Schulz, S. Páll, J. C. Smith, B. Hess, E. Lindahl, *SoftwareX* **2015**, *1 – 2*, 19 – 25.

[29] G. Bussi, D. Donadio, M. Parrinello, *J. Chem. Phys.* **2007**, *126*, 014101.

[30] T. Darden, D. York, L. Pedersen, *J. Chem. Phys.* **1993**, *98*, 10089 – 10092.

[31] B. Hess, H. Bekker, H. J. C. Berendsen, J. G. E. M. Fraaije, *J. Comput. Chem.* **1997**, *18*, 1463 – 1472.

Manuscript received: September 10, 2020
Revised manuscript received: November 9, 2020
Accepted manuscript online: November 11, 2020
Version of record online: December 23, 2020

